Mechanism and Machine Theory 143 (2020) 103616

Contents lists available at ScienceDirect

Mechanism and Machine Theory

journal homepage: www.elsevier.com/locate/mechmachtheory

Research paper

Dynamics of luffing motion of a flexible knuckle boom crane actuated by hydraulic cylinders

Andrej Cibicik[a,*], Eilif Pedersen[b], Olav Egeland[a]

[a] Department of Mechanical and Industrial Engineering, Norwegian University of Science and Technology (NTNU), Trondheim NO-7491, Norway

[b] Department of Marine Technology, Norwegian University of Science and Technology (NTNU), Trondheim NO-7491, Norway

ARTICLE INFO

Article history:
Received 9 July 2019
Revised 30 August 2019
Accepted 9 September 2019
Available online xxx

Keywords:
Crane
Dynamic modeling
Hydraulic cylinder
Reaction force
Screw theory
Bond graph

ABSTRACT

In this paper we present a modeling procedure for a flexible knuckle boom crane, which is actuated by hydraulic cylinders and is modeled as a planar multibody system. We propose a convenient framework where both rigid body velocities and velocities caused by flexible behavior are represented as twists. Such formulation allows for using screw transformations, which leads to systematic derivations. Dynamics of a crane and mass balance of hydraulic cylinders are coupled using the bond graph method. In addition, we present a procedure for the determination of reaction forces in passive joints, which is conveniently given as an extension of the dynamic modeling procedure. Both procedures are presented in a general and systematic manner such that they can be applied for a group of planar flexible manipulators.

We study the dynamics of luffing motion of a crane by numerical simulation and provide the simulation results, as well as determine the reaction forces in passive joints. The simulation results are validated by the ANSYS finite element analysis. The derived model provides a basis for design of luffing cylinders and can potentially be used for studying performance of a crane control system.

1. Introduction

Hoisting of a crane payload is a very common procedure in offshore operations. Safety during the payload landing is an important issue, where the information about the exact position of a payload relative to the landing site is necessary. At the same time there is a limitation for the mass of a crane installed on a smaller supply vessels due to the vessel stability considerations. In such cases lightweight cranes actuated by hydraulic cylinders may be a preferred option. Flexibility of lightweight and long-reach cranes is often significant, which makes it more difficult to operate a crane and estimate the position of a payload. In a mechanical design process of such cranes the internal reaction forces obtained from a dynamic analysis may be required. In addition, flexible behavior of a crane can lead to higher forces in hydraulic cylinders and a hydraulic system may require a different design.

* Corresponding author.
E-mail addresses: andrej.cibicik@ntnu.no (A. Cibicik), eilif.pedersen@ntnu.no (E. Pedersen), olav.egeland@ntnu.no (O. Egeland).

https://doi.org/10.1016/j.mechmachtheory.2019.103616
0094-114X/

Cranes are often modeled as rigid multibody systems [1] due to high stiffness of crane elements. However in some applications flexibility becomes important and several researchers investigated elastic behavior of cranes. Mobile cranes are typical mechanisms where the flexible behavior was investigated. The dynamic model of a mobile crane with a flexible boom was presented in [2], while the dynamic model of a mobile crane with flexibility in the supporting system was presented in [3]. In the other paper [4] the author presented the analysis of flexibility properties of a mobile crane depending on the different selection of flexible components. Another dynamic model of a flexible mobile crane actuated by hydraulic cylinders was presented in [5], where the method of Langrange's multipliers was used for constraining bodies in the system. Alternatively to mobile cranes, flexible behavior of other crane types was also under research. The dynamic response of a tower crane due to the payload motion was presented in [6], where the finite element modeling approach was used. The analysis of an H-type gantry crane, where the transverse beam was modeled as an elastic body, was presented in [7]. A number of flexible cranes actuated by hydraulic cylinders was also investigated. For example, comparison of different methods for modeling a telescopic crane with flexible links was presented in [8], where the crane was actuated by hydraulic cylinders. The dynamic analysis of luffing motion of a flexible single-boom crane actuated by hydraulic cylinders was given in [9].

Knuckle boom cranes are mechanically similar to robotic manipulators, and dynamics of a crane can be formulated in the same manner as dynamics of a robotic manipulator. One of the commonly used methods for modeling dynamics of manipulators is the Euler-Lagrange's formulation [10]. Formulation of velocities and angular velocities as twists can be beneficial for derivation of kinetic energy in Euler-Lagrange's formulation [11,12], as twists satisfy screw transformations, which leads to a general and systematic derivation procedure. It is noted that methods such as the Newton-Euler formulation [13,14] or Kane's equation of motion [15–18] are also commonly used for modeling dynamics of both rigid and flexible multibody systems. A review and comparison of different computational algorithms for solving rigid and flexible multibody dynamics problems was given in [19]. For determination of reaction forces in a dynamical system the method of auxiliary generalized speeds can be used [15]. The method of auxiliary generalized speeds was formulated for rigid body systems using twists and projection matrices in [20], which resulted in a general and systematic procedure. Alternatively, when equations of motion for a multibody system are formulated using the method of Langrange's multipliers as in [21,22], the reaction forces associated with the constrain equations are the unknowns in the system of differential-algebraic equations and are obtained directly.

The bond graph (BG) method [23] is a component-based approach for modeling multiphysical systems, where the energy is exchanged between the components through the bonds. The BG method also allows for convenient graphical representation of a system. The BG method can be used for modeling rigid mechanical systems [24–26], or flexible mechanical systems, as in [27] where a bond graph model of a flexible rotation beam was presented. In [28] the authors presented the bond graph approach for modeling a flexible robot. Since the BG method provides a convenient framework for modeling multiphysical systems [29,30], it can efficiently be applied for modeling dynamics of mechanical systems with hydraulic actuators. The BG model of a rigid knuckle boom crane actuated by hydraulic cylinders was presented in [31], where the authors additionally implemented the functional mock-up interface for the simulation of the system. In [32] the BG model of a hydraulically actuated excavator was presented. In addition, bond graph models of multibody systems actuated by hydraulic motors were discussed in [33].

In this work we extend the previous results of [17,18,20] to the model of a planar flexible knuckle boom crane, which is actuated by hydraulic cylinders. The modeling procedure is given in a generalized and systematic manner, such that it can be applied for a group of planar flexible manipulators. We propose a unified framework for derivation of differential kinematics, where twists are used for formulation of both rigid body velocities and velocities related to flexible behavior. This allows for using screw transformations for flexible multibody systems, which simplifies the derivations. The original formulation of projection matrices [18] for rigid multibody systems is also extended for a case of planar flexible systems. Projection matrices are used for the formulation of the momentum form of Euler–Lagrange's equation [23]. The elasticity of links is modeled using the Euler–Bernoulli beam theory and the assumed mode method. The dynamical model of the crane is coupled with the dynamics of the cylinders using the bond graph method. Additionally, we present a procedure for the determination of reaction forces in passive joints of the crane. The procedure is given as an extension of the dynamic modeling procedure.

We implement the presented procedures numerically and study dynamics of luffing motion by simulations. Simulation results are validated by the finite element analysis in ANSYS. Theoretical results of this work have a potential for practical applications for dimensioning of luffing cylinders, mechanical design of cranes and studying the performance of crane control systems.

The rest of this paper is organized as follows. In Section 2 preliminaries on dynamic modeling of rigid body systems and dynamics of hydraulic cylinders are given. The proposed modeling procedure for flexible planar manipulators is given in Section 3, while coupling of manipulator dynamics and dynamics of hydraulic cylinders using the BG method is presented in Section 4. A procedure for the determination of reaction forces in passive joints is given in Section 5. A numerical example of a knuckle boom crane and simulation results are presented in Section 6, while the conclusions of this work are given in Section 7.

2. Preliminaries

2.1. Twists

Consider a homogeneous transformation matrix $\mathbf{T}_j^i \in \mathrm{SE}(3)$ [34] describing the displacement of Frame j relative to Frame i

$$\mathbf{T}_j^i = \begin{bmatrix} \mathbf{R}_j^i & \mathbf{p}_{ij}^i \\ \mathbf{0}^{\mathrm{T}} & 1 \end{bmatrix}, \tag{1}$$

where $\mathbf{R}_j^i$ is the rotation matrix from Frame i to Frame j [34] and and $\mathbf{p}_{ij}^i$ is the vector from the origin of Frame i to the origin of Frame j given in the coordinates of i. The time derivative of (1) is then given as

$$\dot{\mathbf{T}}_j^i = \mathbf{T}_j^i \hat{\mathrm{t}}_{ij/j}^j, \tag{2}$$

where

$$\hat{\mathrm{t}}_{ij/j}^j = \begin{bmatrix} \hat{\boldsymbol{\omega}}_{ij}^j & \mathbf{v}_{ij/j}^j \\ \mathbf{0}^{\mathrm{T}} & 0 \end{bmatrix} \in \mathrm{se}(3) \tag{3}$$

is the body velocity [35], which can also be called the right velocity. The hat notation $\hat{\cdot}$ refers to a skew-symmetric form of a vector. The body velocity can be represented as a twist vector [36]

$$\mathrm{t}_{ij/j}^j = \left[(\boldsymbol{\omega}_{ij}^j)^{\mathrm{T}} \quad (\mathbf{v}_{ij/j}^j)^{\mathrm{T}} \right]^{\mathrm{T}} \in \mathbb{R}^6. \tag{4}$$

The body velocity of a composite homogeneous transformation $\mathbf{T}_k^i = \mathbf{T}_j^i \mathbf{T}_k^j$ is given as

$$\hat{\mathrm{t}}_{ik/k}^k = [\mathbf{T}_k^i]^{-1} \dot{\mathbf{T}}_k^i = [\mathbf{T}_k^j]^{-1} [\mathbf{T}_j^i]^{-1} \dot{\mathbf{T}}_j^i \mathbf{T}_k^j + [\mathbf{T}_k^j]^{-1} \dot{\mathbf{T}}_k^j = \hat{\mathrm{t}}_{ij/k}^k + \hat{\mathrm{t}}_{jk/k}^k,$$

which leads to

$$\mathrm{t}_{ik/k}^k = \mathrm{t}_{ij/k}^k + \mathrm{t}_{jk/k}^k, \tag{5}$$

which means that the twists referenced to the same point and expressed in the coordinates of the same frame can be summed up. Assume a particular case when Frame i and j are fixed in links of a serial manipulator with one rotational DOF (degree of freedom) in each joint, then the twist (4) can be given as

$$\mathrm{t}_{ij/j}^j = u_j \mathrm{L}_{j/j}^j, \tag{6}$$

where u_j is the generalized speed [16] of Joint j and $\mathrm{L}_{j/j}^j$ is the line of Joint j referenced to j and expressed in the coordinates of j, which is given as

$$\mathrm{L}_{j/j}^j = \left[(\mathbf{a}_j^j)^{\mathrm{T}} \quad (\mathbf{m}_{j/j}^j)^{\mathrm{T}} \right]^{\mathrm{T}}. \tag{7}$$

The term $\mathbf{a}_j^j$ is the axis the line and $\mathbf{m}_{j/j}^j$ is the moment of the line [37], both given in the coordinates of j. From (6) it follows that the twist (4) is a line, which is given as a screw in Plücker coordinates. The line (7) can be transformed to be referenced to the origin of Frame k as

$$\mathrm{L}_{j/k}^j = \mathbf{U}_{k,j}^j \mathrm{L}_{j/j}^j, \tag{8}$$

where $\mathbf{U}_{k,j}^j$ is a screw reference transformation matrix [17] given as

$$\mathbf{U}_{k,j}^j = \begin{bmatrix} \mathbf{I} & \mathbf{0} \\ \hat{\mathbf{p}}_{k,j}^j & \mathbf{I} \end{bmatrix}. \tag{9}$$

The term $\hat{\mathbf{p}}_{k,j}^j$ is a skew-symmetric form of the vector from the origin of Frame k to the origin of Frame j. The line (8) can be expressed in the coordinates of k by the screw coordinate transformation

$$\mathrm{L}_{j/k}^k = \bar{\mathbf{R}}_j^k \mathrm{L}_{j/k}^j, \tag{10}$$

where $\bar{\mathbf{R}}_j^k$ is a screw coordinate transformation matrix [17]

$$\bar{\mathbf{R}}_j^k = \begin{bmatrix} \mathbf{R}_j^k & \mathbf{0} \\ \mathbf{0} & \mathbf{R}_j^k \end{bmatrix} \tag{11}$$

and $\mathbf{R}_j^k \in \mathrm{SO}(3)$ is an orthogonal rotation matrix. The simultaneous coordinate and reference transformation can be generalized by the new notation

$$\mathbf{V}_{k,j}^{k,j} = \bar{\mathbf{R}}_j^k \mathbf{U}_{k,j}^j, \tag{12}$$

such that $\mathsf{L}^k_{j/k} = \mathbf{V}^{k,j}_{k,j}\mathsf{L}^j_{j/j}$. It is noted that the screw transformation $\mathbf{V}^{k,j}_{k,j}$ is equivalent to the adjoint map in SE(3) [11]. We say that $\mathbf{V}^{k,j}_{k,j}$ is a screw transformation matrix which transforms coordinates from j to k and changes the reference point from j to k. The twist (6) when referenced to k and given in the coordinates of k can then be given as

$$\mathsf{t}^k_{ij/k} = u_j \mathsf{L}^k_{j/k}. \tag{13}$$

2.2. Wrenches

A wrench is a screw representation of forces and torques which is given as

$$\mathsf{w}^j_{j/j} = \begin{bmatrix} \mathbf{f}^j_j \\ \mathbf{n}^j_{j/j} \end{bmatrix}, \tag{14}$$

where $\mathbf{f}^j_j$ is a force applied at the origin of Frame j and $\mathbf{n}^j_{j/j}$ is a torque applied at j and referenced to j. The wrench (14) can be formulated as a product of the matrix $\mathbf{L}^j_{j/j}$ and the vector of magnitudes $\boldsymbol{\rho}_r$ as [18]

$$\mathsf{w}^j_{j/j} = \mathbf{L}^j_{j/j}\boldsymbol{\rho}_r, \tag{15}$$

where the vector of force and torque magnitudes is given as

$$\boldsymbol{\rho}_r = \begin{bmatrix} \rho_{f_x} & \rho_{f_y} & \rho_{f_z} & \rho_{n_x} & \rho_{n_y} & \rho_{n_z} \end{bmatrix}^{\mathrm{T}} \tag{16}$$

and the matrix $\mathbf{L}^j_{j/j}$ is referred to as an orthogonal screw basis, which is given as

$$\mathbf{L}^j_{j/j} = \begin{bmatrix} \mathsf{L}^j_{x_j/j} & \mathsf{L}^j_{y_j/j} & \mathsf{L}^j_{z_j/j} & \mathsf{N}^j_{x_j/j} & \mathsf{N}^j_{y_j/j} & \mathsf{N}^j_{z_j/j} \end{bmatrix}, \tag{17}$$

where the lines $\mathsf{L}^j_{a_j/j}$ along the a_j axis and the screws of infinite pitch $\mathsf{N}^j_{a_j/j}$ in the direction of the a_j axis are

$$\begin{aligned}
\mathsf{L}^j_{x_j/j} &= \begin{bmatrix} 1 & 0 & 0 & \mathbf{0}_{1\times 3} \end{bmatrix}^{\mathrm{T}}, \quad \mathsf{N}^j_{x_j/j} = \begin{bmatrix} \mathbf{0}_{1\times 3} & 1 & 0 & 0 \end{bmatrix}^{\mathrm{T}}, \\
\mathsf{L}^j_{y_j/j} &= \begin{bmatrix} 0 & 1 & 0 & \mathbf{0}_{1\times 3} \end{bmatrix}^{\mathrm{T}}, \quad \mathsf{N}^j_{y_j/j} = \begin{bmatrix} \mathbf{0}_{1\times 3} & 0 & 1 & 0 \end{bmatrix}^{\mathrm{T}}, \\
\mathsf{L}^j_{z_j/j} &= \begin{bmatrix} 0 & 0 & 1 & \mathbf{0}_{1\times 3} \end{bmatrix}^{\mathrm{T}}, \quad \mathsf{N}^j_{z_j/j} = \begin{bmatrix} \mathbf{0}_{1\times 3} & 0 & 0 & 1 \end{bmatrix}^{\mathrm{T}}.
\end{aligned} \tag{18}$$

All the columns of (17) are screws, which means that the matrix $\mathbf{L}^j_{j/j}$ satisfies screw transformations. The wrench (14) when referenced to i and expressed in the coordinates of i can be given as

$$\mathsf{w}^i_{j/i} = \mathbf{L}^i_{j/i}\boldsymbol{\rho}_r, \tag{19}$$

where

$$\mathbf{L}^i_{j/i} = \mathbf{V}^{i,j}_{i,j}\mathbf{L}^j_{j/j} \tag{20}$$

and $\mathbf{V}^{i,j}_{i,j}$ is a screw transformation matrix.

2.3. Projection matrices for rigid serial manipulators

Projection matrices for rigid manipulators were discussed in detail in [17], where they were used in combination with Kane's dynamic formulation [15] to represent partial velocities and partial angular velocities as screws in Plücker coordinates. Consider the twist of Link i relative to the inertial frame (Frame 0), referenced to the COG (center of gravity) of Link i and expressed in the coordinates of i, which is given as a sum

$$\mathsf{t}^i_{0i/m_i} = \mathsf{t}^i_{01/m_i} + \cdots + \mathsf{t}^i_{i-1,i/m_i}, \tag{21}$$

which can alternatively be written as

$$\mathsf{t}^i_{0i/m_i} = \sum_{j=1}^{i} u_j \mathsf{L}^i_{j/m_i}, \tag{22}$$

where $\mathsf{L}^i_{j/m_i} = \mathbf{V}^{i,j}_{m_i,j}\mathsf{L}^j_{j/j}$. The expression (22) can also be given in a compact matrix form

$$\mathsf{t}^i_{0i/m_i} = \mathbf{P}^i_{0i/m_i}\mathbf{u}. \tag{23}$$

The term $\mathbf{P}^i_{0i/m_i}$ is referred to as a projection matrix given as

$$\mathbf{P}^i_{0i/m_i} = \begin{bmatrix} \mathsf{L}^i_{1/m_i} & \cdots & \mathsf{L}^i_{i/m_i} & \mathbf{0}_{6\times(n_q-i)} \end{bmatrix}, \tag{24}$$

while $\mathbf{u} = [u_1 \ \ldots \ u_{n_q}]^{\mathrm{T}}$ is the vector of generalized speeds.

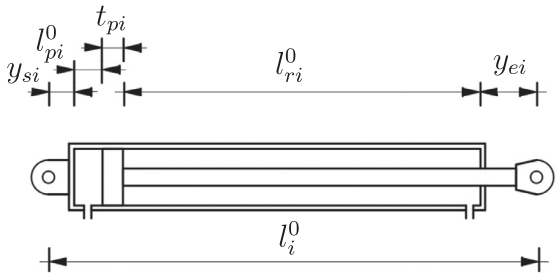

Fig. 1. Geometry of a cylinder i in a fully retracted position. The subscript $\cdot^0$ indicates the value of a variable in a fully retracted position.

2.4. Dynamics of hydraulic cylinders

The continuity equation for a control volume V can be written in a general form as [38,39]

$$\sum \dot{m}_{in} - \sum \dot{m}_{out} = \frac{d}{dt}(\rho_f V) = \dot{\rho}_f V + \rho_f \dot{V}, \tag{25}$$

where $\dot{m}_{in/out} = \rho_f Q_{in/out}$ is the mass flow rate, $Q_{in/out}$ is the volumetric in-flow and out-flow rate, ρ_f is the density of the fluid and V is the control volume. Assume that the temperature is constant and the fluid is compressible with the bulk modulus β, such that the equation of state is

$$\rho_f = \rho_{f0} + \frac{\rho_{f0}}{\beta} p, \tag{26}$$

where ρ_{f0} is the density at zero pressure. Then by substituting (26) into (25) the continuity equation can be formulated as

$$\frac{V}{\beta}\dot{p} + \dot{V} = \sum Q_{in} - \sum Q_{out}, \tag{27}$$

where p is the pressure.

Consider a hydraulic cylinder i shown in Fig. 1. The total length of the cylinder is $l_i = l_i^0 + s_i$, where l_i^0 is the length of the cylinder in a fully retracted position and s_i is the stroke. The volume of the chamber on the piston side is $V_{pi} = A_{pi}(l_{pi}^0 + s_i)$, where A_{pi} is the area of the piston, l_{pi}^0 is the length of the chamber in a fully retracted position. The volume of the chamber on the rod side is $V_{ri} = A_{ri}(l_{ri}^0 - s_i)$, where A_{ri} is the area of the piston subtracted the area of the rod, l_{ri}^0 is the length of the chamber in a fully retracted position. The thickness of the piston is t_{pi}, the offset of the cylinder attachment in the start is y_{si} and the offset of the cylinder attachment in the end is y_{ei}. Assuming that the minimum length of the chamber on the rod side in the fully extended position is limited to l_{ri}^e, then the cylinder stroke is limited to $s_{i,max} = l_{ri}^0 - l_{ri}^e$ and maximum length of the cylinder is $l_{i,max} = l_i^0 + s_{i,max}$.

The dynamics (27) can be written explicitly for the chambers on the piston and rod sides of a hydraulic cylinder as

$$\begin{aligned}
\frac{V_{pi}}{\beta}\dot{P}_{pi} + A_{pi}\dot{s}_i &= -C_{in,i}(P_{pi} - P_{ri}) - C_{ex,i}P_{pi} + Q_{pi}, \\
\frac{V_{ri}}{\beta}\dot{P}_{ri} - A_{ri}\dot{s}_i &= -C_{in,i}(P_{ri} - P_{pi}) - C_{ex,i}P_{ri} + Q_{ri},
\end{aligned} \tag{28}$$

where $C_{in,i}$ is the internal leakage factor and $C_{ex,i}$ is the external leakage factor. The hydraulic flows into chambers on the piston and rod sides can be defined by a directional control valve orifice equation

$$Q_{pi} = \begin{cases} \alpha_i \text{sign}(P_s - P_{pi})\sqrt{|P_s - P_{pi}|}x_{vi}, & \text{if } x_{vi} \geq 0 \\ \alpha_i \text{sign}(P_{pi} - P_r)\sqrt{|P_{pi} - P_r|}x_{vi}, & \text{if } x_{vi} < 0 \end{cases} \tag{29}$$

and

$$Q_{ri} = \begin{cases} -\alpha_i \text{sign}(P_{ri} - P_r)\sqrt{|P_{ri} - P_r|}x_{vi}, & \text{if } x_{vi} \geq 0 \\ -\alpha_i \text{sign}(P_s - P_{ri})\sqrt{|P_s - P_{ri}|}x_{vi}, & \text{if } x_{vi} < 0 \end{cases}, \tag{30}$$

where P_s is the supply pressure, P_r is the pressure in the return reservoir, x_{vi} is the stroke of the valve and α_i is defined as

$$\alpha_i = C_d w_i \sqrt{2/\rho_o}, \tag{31}$$

where C_d is the discharge coefficient, w_i is the relative opening area of the valve orifice and ρ_o is the density of hydraulic oil. We assume a linear proportional valve and w_i is selected such that for $\|x_{vi}\| = 1$ the maximum area of the valve orifice is achieved.

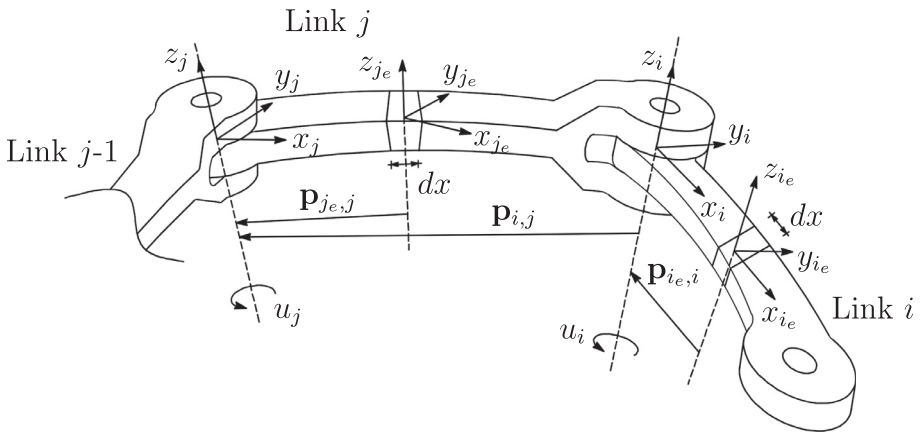

Fig. 2. Flexible manipulator links connected with rotational joints. To simplify the notations Link $j+1$ is denoted Link i.

3. Modeling of planar flexible manipulators

A knuckle boom crane is a mechanical system similar to a robotic manipulator arm. Therefore, in this section we will present the dynamic modeling procedure in a general manner, such that it can be applied for a group of planar flexible mechanical manipulators. The dynamic modeling procedure is given as an extension of [17], where rigid multibody systems were discussed. The elasticity of links is modeled using the Euler-Bernoulli beam theory and the assumed mode method.

3.1. Kinematics

Consider a planar serial flexible manipulator with no actuation torques in the joints. A two-link part of such manipulator is given in Fig. 2. Each elastic Link i has a body-fixed Frame i attached at the end connected to Link $i-1$ and a body-fixed Frame i_e attached at some cross-section located at a distance x from i, when Link i is underformed. Link i has the cross-sectional area $A_i(x)$ and second moment of area $I_i(x)$. The density of the link material is ρ_i and the modulus of elasticity is E_i. Configuration of the manipulator is defined by the vector of generalized coordinates, and the generalized speeds are given by the vector of generalized speeds as

$$\begin{aligned}\mathbf{q} &= \begin{bmatrix} q_1 & \dots & q_{n_q} & (\mathbf{q}^{b1})^{\mathrm{T}} & \dots & (\mathbf{q}^{bn_q})^{\mathrm{T}} \end{bmatrix}^{\mathrm{T}},\\ \mathbf{u} &= \begin{bmatrix} u_1 & \dots & u_{n_q} & (\mathbf{u}^{b1})^{\mathrm{T}} & \dots & (\mathbf{u}^{bn_q})^{\mathrm{T}} \end{bmatrix}^{\mathrm{T}},\end{aligned} \tag{32}$$

where $\mathbf{q}^{bi}$ are the generalized coordinates associated with the assumed modes of elastic deformation of Link i and $u_i = \dot{q}_i$. The twist of Frame i_e relative to the inertial frame, referenced to i_e and given in the coordinates of i can be given as a sum of twists

$$\mathrm{t}^i_{0i_e/i_e} = \sum_{j=1}^{i} \mathrm{t}^i_{j-1,j/i_e} + \mathrm{t}^i_{i,i_e/i_e}, \tag{33}$$

which alternatively can be expressed as

$$\mathrm{t}^i_{0i_e/i_e} = \sum_{j=1}^{i} u_j \mathsf{L}^i_{j/i_e} + \mathbf{S}^i_{i_e/i_e}\mathbf{u}^{bi}, \tag{34}$$

where

$$\mathsf{L}^i_{j/i_e} = \mathbf{V}^{i,j}_{i_e,j}\mathsf{L}^j_{j/j} \tag{35}$$

and

$$\mathbf{S}^i_{i_e/i_e} = \begin{bmatrix} \mathsf{L}^i_{z_i/i}\mathbf{n}_\psi & \mathsf{N}^i_{y_i/i}\mathbf{n}_\psi \end{bmatrix} \begin{bmatrix} \mathrm{diag}[\theta^{bi}_1(x), \dots, \theta^{bi}_{n_\psi}(x)] \\ \mathrm{diag}[\psi^{bi}_1(x), \dots, \psi^{bi}_{n_\psi}(x)] \end{bmatrix}, \tag{36}$$

where $\mathbf{n}_\psi = [1 \ \dots \ 1]$, $\psi^{bi}_k(x)$ is the k-th assumed mode of Link i evaluated at x and $\theta^{bi}_k(x) = \partial\psi^{bi}_k(x)/\partial x$. The line $\mathsf{L}^i_{z_i/i}$ and the screw $\mathsf{N}^i_{y_i/i}$ are given in (18). The twist (34) can be written in a compact matrix form as

$$\mathrm{t}^i_{0i_e/i_e} = \mathbf{P}^i_{0i_e/i_e}\mathbf{u}, \tag{37}$$

where the projection matrix of the elastic Link i is given as

$$\mathbf{P}^i_{0i_e/i_e} = \begin{bmatrix} \mathsf{L}^i_{1/i_e} & \cdots & \mathsf{L}^i_{i/i_e} & \mathbf{0}_{6\times(n_q-i)} & \mathbf{0}_{6\times(n_\psi(i-1))} & \mathbf{S}^i_{i_e/i_e} & \mathbf{0}_{6\times(n_\psi(n_q-i))} \end{bmatrix}, \tag{38}$$

where n_q is the number of links in the manipulator and n_ψ is the number of assumed modes for modeling the flexibility of each link.

3.2. Dynamics of flexible manipulators

In this section we derive a momentum form of equation of motion [23]. Such representation makes it straightforward to implement dynamics in the bond graph framework in the next section. The kinetic energy of the cross-section i_e of Link i can be given in terms of the twist $\mathsf{t}^i_{0i_e/i_e}$ as

$$\mathcal{T}_{i_e} = \frac{1}{2}(\mathsf{t}^i_{0i_e/i_e})^{\mathrm{T}}\mathbf{D}_{ei}\mathsf{t}^i_{0i_e/i_e} = \frac{1}{2}\mathbf{u}^{\mathrm{T}}\Big[(\mathbf{P}^i_{0i_e/i_e})^{\mathrm{T}}\mathbf{D}_{ei}\mathbf{P}^i_{0i_e/i_e}\Big]\mathbf{u}, \tag{39}$$

where (37) is used,

$$\mathbf{D}_{ei} = \begin{bmatrix} \rho_i\mathbf{J}^i_{i_e} & \mathbf{0} \\ \mathbf{0} & \rho_i A_i\mathbf{I} \end{bmatrix} \tag{40}$$

and $\mathbf{J}^i_{i_e}$ is the matrix of second moments of area for a cross-section at i_e. The kinetic energy of the whole manipulator given in terms of the generalized coordinates is

$$\mathcal{T} = \frac{1}{2}\sum_i \int_0^{L_i} \mathcal{T}_{i_e}\, dx = \frac{1}{2}\mathbf{u}^{\mathrm{T}}\Big[\sum_i \int_0^{L_i} (\mathbf{P}^i_{0i_e/i_e})^{\mathrm{T}}\mathbf{D}_{ei}\mathbf{P}^i_{0i_e/i_e}\, dx\Big]\mathbf{u} = \frac{1}{2}\mathbf{u}^{\mathrm{T}}\mathbf{M}\mathbf{u}, \tag{41}$$

where the mass matrix is formulated as

$$\mathbf{M} = \sum_i \int_0^{L_i} (\mathbf{P}^i_{0i_e/i_e})^{\mathrm{T}}\mathbf{D}_{ei}\mathbf{P}^i_{0i_e/i_e}\, dx. \tag{42}$$

The equation of motion can then be given in terms of momentum [23] as

$$\dot{\mathbf{p}} - \mathbf{E} + \mathbf{K} = \mathbf{G} + \boldsymbol{\tau}, \tag{43}$$

where $\mathbf{p} = \mathbf{M}\mathbf{u}$ and the generalized forces associated with the derivative of kinetic energy with respect to the generalized coordinates are given as

$$\mathbf{E} = \frac{\partial \mathcal{T}}{\partial \mathbf{q}}, \tag{44}$$

where $\mathcal{T}$ is given by (41) and $\mathbf{q}$ is given by (32). The vector of generalized gravitational forces is given by

$$\mathbf{G} = \sum_i \int_0^{L_i} (\mathbf{P}^i_{0i_e/i_e})^{\mathrm{T}}\boldsymbol{\Pi}\mathsf{w}^{i(g)}_{i_e/i_e}\, dx, \tag{45}$$

the matrix $\boldsymbol{\Pi}$ is an interchange operator [36] given as

$$\boldsymbol{\Pi} = \begin{bmatrix} \mathbf{0} & \mathbf{I} \\ \mathbf{I} & \mathbf{0} \end{bmatrix} \tag{46}$$

and $\mathsf{w}^{i(g)}_{i_e/i_e}$ is the wrench of gravitational forces applied at the origin of Frame i_e, referenced to i_e and given in the coordinates of i

$$\mathsf{w}^{i(g)}_{i_e/i_e} = \bar{\mathbf{R}}^i_0\mathsf{w}^{0(g)}_{i_e/i_e}, \tag{47}$$

where $\bar{\mathbf{R}}^i_0$ is a screw coordinate transformation matrix (11) and

$$\mathsf{w}^{0(g)}_{i_e/i_e} = \begin{bmatrix} 0 & -\rho_i A_i g & 0 & 0 & 0 & 0 \end{bmatrix}^{\mathrm{T}}, \tag{48}$$

when the gravity force acts in the negative y_0 direction of the inertial frame. The vector of generalized actuation forces is given as

$$\boldsymbol{\tau} = \sum_i \int_0^{L_i} (\mathbf{P}^i_{0i_e/i_e})^{\mathrm{T}}\boldsymbol{\Pi}(\mathsf{w}^i_{h_{i.1}/h_{i.1}} + \mathsf{w}^i_{h_{i.2}/h_{i.2}})\, dx, \tag{49}$$

where the wrenches of external actuation forces $\mathsf{w}^i_{h_{i,x}/h_{i,x}}$ applied at the point $H_{i,x}$, referenced to $H_{i,x}$ and expressed in the coordinates of i will be defined in the next section.

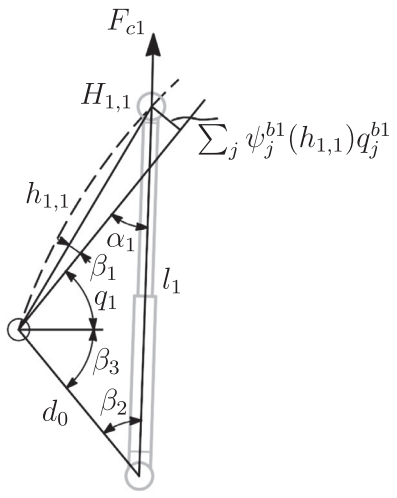

(a) Connection of actuator 1 to Link 1. The dashed line shows the deformed axis of Link 1, while the solid line shows the undeformed axis.

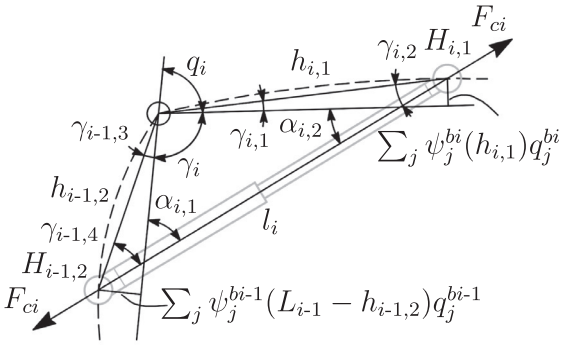

(b) Connection of actuator i to Link $i-1$ and Link i. The dashed lines show the deformed axes of Links $i-1$ and i, while the solid lines show the undeformed axes.

Fig. 3. Geometry of actuators connected to deformed manipulator links.

The elastic strain energy for Link i, which is modeled as an Euler-Bernoulli beam, is formulated as

$$U_i = \frac{1}{2}E_i \int_0^{L_i} I_i(x)\left[\frac{\partial \theta_i(x,t)}{\partial x}\right]^2 dx, \tag{50}$$

where θ_i is the elastic rotation of i_e. The generalized restoring forces associated with elastic deformation are determined as partial derivatives of the strain energy with respect to the generalized coordinates, which leads to the following definition of the stiffness matrix

$$\mathbf{K} = \sum_i E_i \int_0^{L_i} I_i(x)(\mathbf{\Theta}_i')^{\mathrm{T}}\mathbf{\Theta}_i' \, dx, \tag{51}$$

where $\mathbf{\Theta}_i' = \partial\theta_i'/\partial\mathbf{q}$ and $\theta_i' = \partial\theta_i/\partial x$.

3.3. Magnitudes of linear actuator forces

3.3.1. Linear actuator of Link 1

Assume that the curved geometry of the segment between the origin of Frame 1 and the point $H_{1,1}$ is approximated by a straight line, see Fig. 3(a). Then the angle β_1 is defined by the sine rule as

$$\beta_1 = \arcsin\left[\frac{\sum_j \psi_j^{b1}(h_{1,1})q_j^{b1}}{h_{1,1}}\right]. \tag{52}$$

The length of the actuator l_1 is calculated by the cosine rule as

$$l_1 = \left[d_0^2 + h_{1,1}^2 - 2d_0h_{1,1}\cos(q_1+\beta_1+\beta_3)\right]^{\frac{1}{2}}, \tag{53}$$

where d_0 and $h_{1,1}$ are given in Fig. 3(a). The angle β_2 is defined as

$$\beta_2 = \arcsin\left[\frac{h_{1,1}\sin(q_1+\beta_1+\beta_3)}{l_1}\right] \tag{54}$$

and the angle α_1 is

$$\alpha_1 = \pi - q_1 - \beta_2 - \beta_3. \tag{55}$$

The wrench of the external actuation force from the actuator 1 on Link 1 applied at the point $H_{1,1}$, referenced to $H_{1,1}$ and given in the coordinates of Frame 1 is

$$\mathrm{w}^1_{h_{1,1}/h_{1,1}} = \delta(x-h_{1,1})F_{c1}\begin{bmatrix}\cos(\alpha_1) & \sin(\alpha_1) & 0 & 0 & 0 & 0\end{bmatrix}^{\mathrm{T}}, \tag{56}$$

where F_{c1} is the axial force of the actuator and $\delta(x)$ is the Dirac delta function.

3.3.2. Linear actuators for all other links

As in the previous section, assume that the curved segment between the point $H_{i-1,2}$ and the origin of Frame i, as well as the curved segment between the origin of Frame i and the point $H_{i,1}$ are approximated by straight lines, see Fig. 3(b). Then the angles $\gamma_{i\text{-}1,3}$ and $\gamma_{i,1}$ are defined by the sine rule as

$$\gamma_{i\text{-}1,3} = \arcsin\left[\frac{\sum_j \psi_j^{bi\text{-}1}(L_{i\text{-}1} - h_{i\text{-}1,2})q_j^{bi\text{-}1}}{h_{i\text{-}1,2}}\right], \quad \gamma_{i,1} = \arcsin\left[\frac{\sum_j \psi_j^{bi}(h_{i,1})q_j^{bi}}{h_{i,1}}\right], \tag{57}$$

while the angle γ_i is given as

$$\gamma_i = \pi + q_i, \tag{58}$$

where q_i as shown in Fig. 3(b) has a negative value. The length of the actuator l_i is calculated by the cosine rule as

$$l_i = \left[h_{i\text{-}1,2}^2 + h_{i,1}^2 - 2h_{i\text{-}1,2}h_{i,1}\cos\left(\gamma_{si}\right)\right]^{\frac{1}{2}}, \tag{59}$$

where $h_{i\text{-}1,2}$, $h_{i,1}$ are given in Fig. 3(b) and $\gamma_{si} = \gamma_{i\text{-}1,3} + \gamma_{i,1} + \gamma_i$. The angles $\gamma_{i\text{-}1,4}$ and $\gamma_{i,2}$ are given as

$$\gamma_{i\text{-}1,4} = \arcsin\left[\frac{h_{i,1}\sin(\gamma_{si})}{l_i}\right], \quad \gamma_{i,2} = \arcsin\left[\frac{h_{i\text{-}1,2}\sin(\gamma_{si})}{l_i}\right], \tag{60}$$

then the angles $\alpha_{i,1}$ and $\alpha_{i,2}$ are given as

$$\alpha_{i,1} = \gamma_{i\text{-}1,3} + \gamma_{i\text{-}1,4}, \quad \alpha_{i,2} = \gamma_{i,1} + \gamma_{i,2}. \tag{61}$$

The wrench of the external actuation force from the actuator i on Link $i-1$ applied at the point $H_{i-1,2}$, referenced to $H_{i-1,2}$ and given in the coordinates of Frame $i-1$ is

$$\mathrm{w}^{i-1}_{h_{i\text{-}1,2}/h_{i\text{-}1,2}} = \delta(x - (L_{i\text{-}1} - h_{i\text{-}1,2}))F_{ci}\begin{bmatrix}-\cos(\alpha_{i,1}) & \sin(\alpha_{i,1}) & 0 & 0 & 0 & 0\end{bmatrix}^{\mathrm{T}} \tag{62}$$

and the wrench of the external actuation force from the actuator i on Link i applied at the point $H_{i,1}$, referenced to $H_{i,1}$ and given in the coordinates of Frame i is

$$\mathrm{w}^{i}_{h_{i,1}/h_{i,1}} = \delta(x - h_{i,1})F_{ci}\begin{bmatrix}\cos(\alpha_{i,2}) & \sin(\alpha_{i,2}) & 0 & 0 & 0 & 0\end{bmatrix}^{\mathrm{T}}, \tag{63}$$

where F_{ci} is the axial force of the actuator.

4. Coupling of manipulator and cylinder models using bond graph

The dynamical model of a planar flexible manipulator (43) and the dynamics of a hydraulic cylinder (28) are coupled into one dynamical system using the bong graph method.

4.1. Manipulator model

The equation of motion of a planar flexible manipulator (43) is used for the derivation of the bong graph model in this section. The bond graph model is illustrated in Fig. 5. A reader can refer to [23,40] for a summary of the bond graph elements.

Define the states of the $\mathbf{I}_1$ element as $\mathbf{p}_1 = \int \mathbf{e}_1 dt$ and $\mathbf{q}_2 = \int \mathbf{f}_2 dt$, then the output port variables are found as

$$\mathbf{f}_1 = \mathbf{M}^{-1}\mathbf{p}_1, \quad \mathbf{e}_2 = -\mathbf{E} + \mathbf{D}\mathbf{f}_2, \tag{64}$$

where $\mathbf{D}$ is a diagonal matrix of damping coefficients and $\mathbf{M}$ is given by (42). The effort in the power bond 3 is defined as

$$\mathbf{e}_3 = -\mathbf{G} + \mathbf{K}\int \mathbf{f}_3 dt, \tag{65}$$

where the vector of generalized gravitational forces associated with the manipulator masses $\mathbf{G}$ is given in (45) and the stiffness matrix $\mathbf{K}$ is given in (51). The constitutive relations of the modulated transformer MTF_4^{i12} are defined as

$$\mathbf{e}_4 = \boldsymbol{\tau}_b\begin{bmatrix}e_{112} & \dots & e_{n_q 12}\end{bmatrix}^{\mathrm{T}}, \quad \begin{bmatrix}f_{112} & \dots & f_{n_q 12}\end{bmatrix}^{\mathrm{T}} = \boldsymbol{\tau}_b^{\mathrm{T}}\mathbf{f}_4, \tag{66}$$

where the matrix $\boldsymbol{\tau}_b = \begin{bmatrix}\boldsymbol{\tau}_1 & \dots & \boldsymbol{\tau}_{n_q}\end{bmatrix}$, the vector $\boldsymbol{\tau}_1$ is

$$\boldsymbol{\tau}_1 = \frac{1}{F_{c1}}\int_0^{L_1} (\mathbf{P}^1_{01_e/1_e})^{\mathrm{T}}\boldsymbol{\Pi}\mathrm{w}^1_{h_{1,1}/h_{1,1}}\, dx \tag{67}$$

and the vector $\boldsymbol{\tau}_i$ for $i > 1$ is

$$\boldsymbol{\tau}_i = \frac{1}{F_{ci}}\left[\int_0^{L_{i-1}} (\mathbf{P}^{i-1}_{0(i-1)_e/(i-1)_e})^{\mathrm{T}}\boldsymbol{\Pi}\mathrm{w}^{i-1}_{h_{i-1,2}/h_{i-1,2}}\, dx + \int_0^{L_i} (\mathbf{P}^{i}_{0i_e/i_e})^{\mathrm{T}}\boldsymbol{\Pi}\mathrm{w}^{i}_{h_{i,1}/h_{i,1}}\, dx\right]. \tag{68}$$

The final vector of generalized actuation forces (49) can then alternatively be written as

$$\boldsymbol{\tau} = \boldsymbol{\tau}_b\begin{bmatrix}F_{c1} & \dots & F_{cn_q}\end{bmatrix}^{\mathrm{T}}. \tag{69}$$

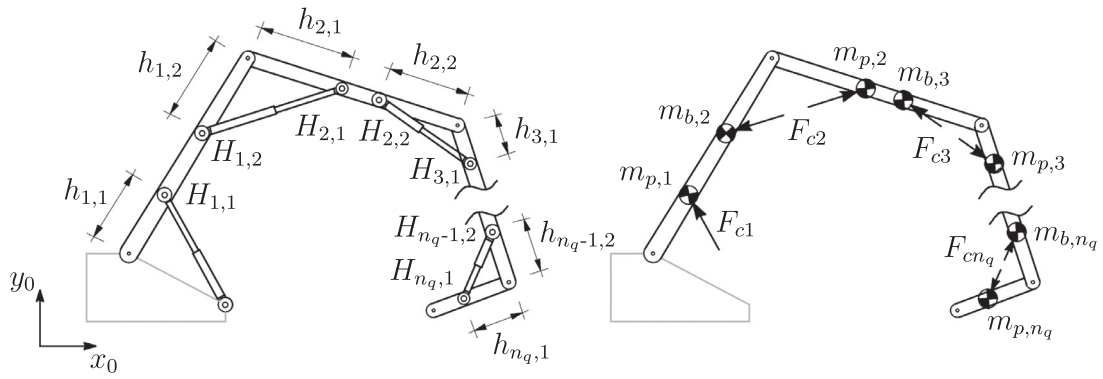

Fig. 4. The mass of actuators is assumed to be lumped on manipulator links, and the forces from actuators are applied on manipulator links. Frame 0 denotes the inertial frame.

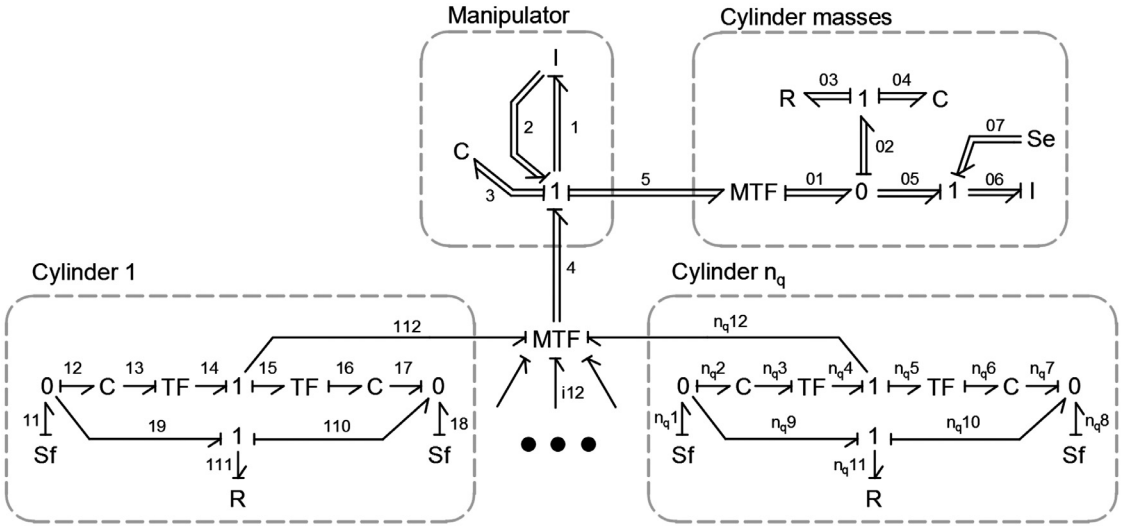

Fig. 5. Bond graph of the flexible manipulator coupled with hydraulic cylinders.

4.2. Cylinder masses

We assume that inertia of cylinders can sufficiently accurately be represented by lumped masses attached to manipulator links, see Fig. 4. This assumption is validated by numerical simulations in Section 6. Each cylinder i consists of a barrel with a mass m_{bi} and a piston with a mass m_{pi}. The masses are connected to the links through the spring-damper system, where the spring stiffness is selected to be sufficient to minimize the relative motion between the links and cylinder masses. The constitutive relations of MTF_{01}^{5} are given as

$$\mathbf{f}_{01} = \mathbf{J}_c \mathbf{f}_5, \quad \mathbf{e}_5 = \mathbf{J}_c^{\mathrm{T}} \mathbf{e}_{01}, \tag{70}$$

where $\mathbf{J}_c$ is a geometric Jacobian, which can conveniently be formulated using projection matrices as

$$\mathbf{J}_c = \begin{bmatrix} \mathbf{N}_c \mathbf{P}^0_{0,h_{1,1}/h_{1,1}} \\ \mathbf{N}_c \mathbf{P}^0_{0,h_{1,2}/h_{1,2}} \\ \mathbf{N}_c \mathbf{P}^0_{0,h_{2,1}/h_{2,1}} \\ \cdots \\ \mathbf{N}_c \mathbf{P}^0_{0,h_{nq,1}/h_{nq,1}} \end{bmatrix}, \tag{71}$$

where

$$\mathbf{N}_c = \begin{bmatrix} \mathbf{0}_{2\times 3} & \mathbf{I}_{2\times 2} & \mathbf{0}_{2\times 1} \end{bmatrix} \tag{72}$$

is the auxiliary matrix which eliminates the zero rows associated with rotational inertia and inertia along the z axis. The projection matrices in (71) are given as

$$\mathbf{P}^0_{0,h_{i,k}/h_{i,k}} = \begin{bmatrix} \mathsf{L}^0_{1/h_{i,k}} & \cdots & \mathsf{L}^0_{i/h_{i,k}} & \mathbf{0}_{6\times(n_q-i)} & \mathbf{0}_{6\times(n_\psi(i-1))} & \mathbf{S}^0_{h_{i,k}/h_{i,k}} & \mathbf{0}_{6\times(n_\psi(n_q-i))} \end{bmatrix}, \tag{73}$$

where $k = 1, 2$, and the line of Joint j referenced to the point $H_{i,1}$ or $H_{i,2}$ on Link i and given in the coordinates of the inertial frame is

$$\mathsf{L}^0_{j/h_{i,1}} = \mathbf{V}^{0,j}_{h_{i,1},j}\mathsf{L}^j_{j/j}, \quad \mathsf{L}^0_{j/h_{i,2}} = \mathbf{V}^{0,j}_{h_{i,2},j}\mathsf{L}^j_{j/j}, \tag{74}$$

where $\mathsf{L}^j_{j/j}$ is the same as in (35). The flow in the power bond 06 is defined as

$$\mathbf{f}_{06} = \mathbf{M}_c^{-1}\int \mathbf{e}_{06}dt, \tag{75}$$

where the mass matrix is $\mathbf{M}_c = \mathrm{diag}(m_{p1}\mathbf{I}_{2\times2}, m_{b2}\mathbf{I}_{2\times2}, m_{p2}\mathbf{I}_{2\times2}, \ldots, m_{pn_q}\mathbf{I}_{2\times2})$. The effort in the bond 07 is the force of gravity which is defined as

$$\mathbf{e}_{07} = -g\begin{bmatrix}0 & m_{p1} & 0 & m_{b2} & 0 & m_{p2} & \ldots & 0 & m_{pn_q}\end{bmatrix}^{\mathrm{T}}, \tag{76}$$

where the inertial frame is oriented as given in Fig. 4. The efforts in the bonds 03 and 04 are defined as

$$\mathbf{e}_{03} = \mathbf{f}_{03}R_{03}, \quad \mathbf{e}_{04} = \frac{1}{C_{04}}\int \mathbf{f}_{04}dt, \tag{77}$$

where R_{04} and C_{04} are the damping and compliance coefficients of the connections between cylinder masses and links.

4.3. Hydraulic model of cylinders

In this section we implement the dynamics of a hydraulic cylinder (28) as a bond graph model. The modeling approach presented in [41] was used as a basis. Consider the dynamics of the hydraulic cylinder i, which is coupled with dynamics of the manipulator by the power bond $i12$, see Fig. 5. Explicit modeling of the hydraulic system is outside the scope of this work. Therefore, a simplified system is considered. The mathematical model of a directional control valve is implemented for controlling the hydraulic oil flow. In this work we disregard the effects of hoses transporting hydraulic oil in the system and external leakages.

The flow in the power bond $i1$ of the flow source Sf is defined by the orifice flow equation (29) where $P_{pi} = e_{i2}$. The flow in the power bond $i8$ of the flow source Sf is defined by (30) where $P_{ri} = e_{i7}$. The efforts in the power bonds $i2$, $i3$ and the efforts in the power bonds $i6$, $i7$ are defined as

$$e_{i2} = e_{i3} = \frac{1}{C_{pi}}\int (f_{i2} - f_{i3})dt, \quad e_{i6} = e_{i7} = \frac{1}{C_{ri}}\int (f_{i7} - f_{i6})dt. \tag{78}$$

The compliance coefficients in (78) are defined as

$$C_{pi} = \frac{V_{pi}}{\beta}, \quad C_{ri} = \frac{V_{ri}}{\beta}, \tag{79}$$

where V_{pi}, V_{ri} are the chamber control volumes on the piston and rod sides respectively and β is the hydraulic oil bulk modulus. The constitutive relations for the transformer TF^{i3}_{i4} are defined as

$$e_{i4} = A_{pi}e_{i3}, \quad f_{i3} = A_{pi}f_{i4}, \tag{80}$$

where A_{pi} is the piston area. The constitutive relations for the transformer TF^{i5}_{i6} are defined as

$$e_{i5} = A_{ri}e_{i6}, \quad f_{i6} = A_{ri}f_{i5}, \tag{81}$$

where A_{ri} is the piston area subtracted the rod area. The resistor element R_{i11} represents the losses due to internal leakage. The flow of the power bond $i11$ is defined as

$$f_{i11} = \frac{e_{i11}}{R_{li}} = \frac{e_{i9} - e_{i10}}{R_{li}}, \tag{82}$$

where R_{li} is the internal leakage coefficient.

The control input of the valve piston x_{vi} is defined by the P (proportional) control law

$$x_{vi} = \begin{cases} -K_{vi}(l_i - l_{id}), & \text{if } |K_{vi}(l_i - l_{id})| \leq 1 \\ -1 \cdot \mathrm{sign}(l_i - l_{id}), & \text{otherwise} \end{cases}, \tag{83}$$

where l_i is given by (53) of (59), l_{id} is the desired value of the cylinder length and the gain K_{vi} is some positive constant.

5. Reaction forces

In this section we present a procedure for the determination of reaction forces in passive joints of a manipulator. The procedure is based on the results in [17,20]. Consider the vector of magnitudes of the unknown reaction forces

$$\boldsymbol{\rho}_r = \begin{bmatrix} \boldsymbol{\rho}_{r1}^{\mathrm{T}} & \cdots & \boldsymbol{\rho}_{rj}^{\mathrm{T}} & \cdots & \boldsymbol{\rho}_{rn_q}^{\mathrm{T}} \end{bmatrix}^{\mathrm{T}}, \tag{84}$$

where for every $\boldsymbol{\rho}_{rj} = [\rho_{rjx}\ \rho_{rjy}]^{\mathrm{T}}$ the magnitudes ρ_{rjx}, ρ_{rjy} correspond to the reaction forces in x and y directions in Joint j given in the coordinates of j. Then the wrench of the reaction forces in the Joint j can be generally given as

$$\mathrm{w}_{j/j}^{(r)j} = \begin{bmatrix} \rho_{rjx} & \rho_{rjy} & 0 & \mathbf{0}_{1\times 3} \end{bmatrix}^{\mathrm{T}}. \tag{85}$$

The wrench (85) can alternatively be written as

$$\mathrm{w}_{j/j}^{(r)j} = \mathbf{L}_{j/j}^{j} \boldsymbol{\rho}_{rj}, \tag{86}$$

where the screw basis matrix $\mathbf{L}_{j/j}^{j}$ is

$$\mathbf{L}_{j/j}^{j} = \begin{bmatrix} \mathrm{L}_{x_j/j}^{j} & \mathrm{L}_{y_j/j}^{j} \end{bmatrix}, \tag{87}$$

where $\mathrm{L}_{x_j/j}^{j}$ and $\mathrm{L}_{y_j/j}^{j}$ are given in (18). Since all columns of (87) are screws, then $\mathbf{L}_{j/j}^{j}$ satisfies screw transformations. The screw basis $\mathbf{L}_{i/i}^{i}$ can be transformed to be referenced to the origin of Frame i_e and expressed in the coordinates of k as

$$\mathbf{L}_{j/i_e}^{k} = \mathbf{V}_{i_e,j}^{k,j} \boldsymbol{\Pi} \mathbf{L}_{j/j}^{j}, \tag{88}$$

where $\boldsymbol{\Pi}$ is given by (46). The auxiliary projection matrix for the Link i is defined as

$$\mathbf{P}_{r,0\mathrm{i}/i_e}^{i} = \begin{bmatrix} \mathbf{L}_{1/i_e}^{i} & \cdots & \mathbf{L}_{i/i_e}^{i} & \mathbf{0}_{6\times(2(n_q-i))} \end{bmatrix}. \tag{89}$$

Similarly we define auxiliary projection matrices for the actuator masses

$$\mathbf{P}_{r,0\mathrm{i}/h_{i,k}}^{0} = \begin{bmatrix} \mathbf{L}_{1/h_{i,k}}^{0} & \cdots & \mathbf{L}_{i/h_{i,k}}^{0} & \mathbf{0}_{6\times(2(n_q-i))} \end{bmatrix}, \quad \text{for } k = 1, 2. \tag{90}$$

The auxiliary matrix of inertial forces is then defined as

$$\mathbf{M}_r = \sum_i \left[\int_0^{L_i} (\mathbf{P}_{r,0\mathrm{i}/i_e}^{i})^{\mathrm{T}} \mathbf{D}_{ei} \mathbf{P}_{0i_e/i_e}^{i} \, dx + (\mathbf{P}_{r,0\mathrm{i}/h_{i,1}}^{0})^{\mathrm{T}} \mathbf{D}_{pi} \mathbf{P}_{0,h_{i,1}/h_{i,1}}^{0} + (\mathbf{P}_{r,0\mathrm{i}/h_{i,2}}^{0})^{\mathrm{T}} \mathbf{D}_{bi} \mathbf{P}_{0,h_{i,2}/h_{i,2}}^{0} \right], \tag{91}$$

where $\mathbf{P}_{0i_e/i_e}^{i}$ is given by (38), $\mathbf{P}_{0,h_{i,k}/h_{i,k}}^{0}$ is given by (73), $\mathbf{D}_{ei}$ is given by (40) and

$$\mathbf{D}_{pi} = \begin{bmatrix} \mathbf{0} & \mathbf{0} \\ \mathbf{0} & m_{pi}\mathbf{I} \end{bmatrix}, \quad \mathbf{D}_{bi} = \begin{bmatrix} \mathbf{0} & \mathbf{0} \\ \mathbf{0} & m_{bi}\mathbf{I} \end{bmatrix}. \tag{92}$$

The auxiliary vector of gravitational forces is defined as

$$\mathbf{G}_r = \sum_i \left[\int_0^{L_i} (\mathbf{P}_{r,0\mathrm{i}/i_e}^{i})^{\mathrm{T}} \boldsymbol{\Pi} \mathrm{w}_{i_e/i_e}^{(g)i} \, dx + (\mathbf{P}_{r,0\mathrm{i}/h_{i,1}}^{0})^{\mathrm{T}} \boldsymbol{\Pi} \mathrm{w}_{h_{i,1}/h_{i,1}}^{(g)0} + (\mathbf{P}_{r,0\mathrm{i}/h_{i,2}}^{0})^{\mathrm{T}} \boldsymbol{\Pi} \mathrm{w}_{h_{i,2}/h_{i,2}}^{(g)0} \right], \tag{93}$$

where $\mathrm{w}_{i_e/i_e}^{(g)i}$ is given by (47) and

$$\mathrm{w}_{h_{i,1}/h_{i,1}}^{(g)0} = \begin{bmatrix} 0 & -m_{pi}g & 0 & 0 & 0 & 0 \end{bmatrix}^{\mathrm{T}}, \quad \mathrm{w}_{h_{i,2}/h_{i,2}}^{(g)0} = \begin{bmatrix} 0 & -m_{b,i+1}g & 0 & 0 & 0 & 0 \end{bmatrix}^{\mathrm{T}}. \tag{94}$$

The auxiliary matrix of normalized actuation forces is given as $\boldsymbol{\tau}_r = \begin{bmatrix} \boldsymbol{\tau}_{r1} & \cdots & \boldsymbol{\tau}_{r,n_q} \end{bmatrix}$, where the vector $\boldsymbol{\tau}_{r1}$ is

$$\boldsymbol{\tau}_{r1} = \frac{1}{F_{c1}} \int_0^{L_1} (\mathbf{P}_{r,01/1_e}^{1})^{\mathrm{T}} \boldsymbol{\Pi} \mathrm{w}_{h_{1,1}/h_{1,1}}^{1} \, dx \tag{95}$$

and the vector $\boldsymbol{\tau}_{ri}$ for $i > 1$ is

$$\boldsymbol{\tau}_{ri} = \frac{1}{F_{ci}} \left[\int_0^{L_{i-1}} (\mathbf{P}_{r,0(i-1)/(i-1)_e}^{i-1})^{\mathrm{T}} \boldsymbol{\Pi} \mathrm{w}_{h_{i-1,2}/h_{i-1,2}}^{i-1} \, dx + \int_0^{L_i} (\mathbf{P}_{r,0\mathrm{i}/i_e}^{i})^{\mathrm{T}} \boldsymbol{\Pi} \mathrm{w}_{h_{i,1}/h_{i,1}}^{i} \, dx \right]. \tag{96}$$

where $\mathrm{w}_{h_{i-1,2}/h_{i-1,2}}^{i-1}$ and $\mathrm{w}_{h_{i,1}/h_{i,1}}^{i}$ are given in (62) and (63). The vector of the unknown magnitudes of the reaction forces can now be determined as

$$\boldsymbol{\rho}_r = \mathbf{M}_r \dot{\boldsymbol{\vartheta}} + \mathbf{G}_r + \boldsymbol{\tau}_r \begin{bmatrix} e_{112} & \cdots & e_{n_q 12} \end{bmatrix}^{\mathrm{T}}, \tag{97}$$

where e_i is the effort in the power bond i and $\mathbf{q}$ are obtained from the dynamic analysis of the system, and

$$\dot{\boldsymbol{\vartheta}} = \mathbf{M}^{-1}(\mathbf{e}_2 - \mathbf{e}_1), \tag{98}$$

where $\mathbf{e}_i$ are the efforts in the power bond i, and $\mathbf{M}$ is given in (42).

(a) A small-scale knuckle boom crane [17].

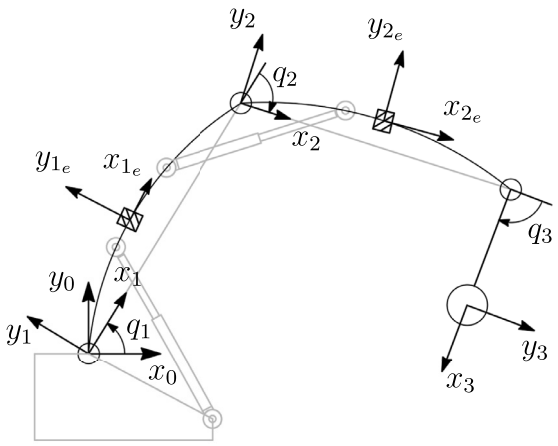

(b) Coordinate frames used in the model.

Fig. 6. A knuckle boom crane.

Table 1
Crane parameters.

Term	L_1	L_2	L_3	d_0	h_1	h_2	h_3
Value, m	10.0	8.0	6.0	3.0	4.0	4.0	3.0
Term	A_1, A_2		I_1, I_2		E	m_3	β_3
Value	0.0264 m^2		$5.89 \cdot 10^{-4}$ m^4		210 GPa	5.0 t	60°

6. Numerical example: A knuckle boom crane

6.1. System description

Consider a knuckle boom crane, which is modeled as a planar system, given in Fig. 6. Link 1 is the main boom of the crane, Link 2 is the knuckle boom of the crane and Link 3 is the payload pendulum. The first two links are modeled as elastic bodies and the payload is modeled as a lumped mass attached to a rigid massless wire. The inertial frame of the system is denoted Frame 0. The body-fixed frame at the start of Link 1 is Frame 1, while Frame 1e is fixed in Link 1 cross-section located at the distance x from the origin of Frame 1 along the x_1 axis, when Link 1 is undeformed. The body-fixed frame at the start of Link 2 is Frame 2, while Frame 2e is fixed in Link 2 cross-section located at the distance x from the origin of Frame 2 along the x_2 axis, when Link 2 is undeformed. The body-fixed frame at the end of Link 3 is Frame 3. The rotation angle of Frame 1 relative to Frame 0 about the z_1 axis is q_1. The rotation angle of Frame 2 relative to Frame 1 about the z_2 axis is q_2. The rotation angle of Frame 3 relative to Frame 2 about the z_3 axis is q_3. The length of Link i is denoted L_i. The cross-sectional area and second moment of area of Link i are assumed to be constant and are denoted A_i and I_i, where $i = 1, 2$. The mass of the payload is m_3, which is located at the origin of Frame 3. Each of two hydraulic cylinders consists of a barrel and a piston with masses m_b and m_p respectively, and both cylinders are assumed to be identical.

The configuration of the system is given by the vector of generalized coordinates

$$\mathbf{q} = \begin{bmatrix} q_1 & q_2 & q_3 & q_1^{b1} & q_2^{b1} & q_3^{b1} & q_1^{b2} & q_2^{b2} & q_3^{b2} \end{bmatrix}^{\mathrm{T}}, \tag{99}$$

while the corresponding vector of generalized speeds [15] is given as

$$\mathbf{u} = \begin{bmatrix} u_1 & u_2 & u_3 & u_1^{b1} & u_2^{b1} & u_3^{b1} & u_1^{b2} & u_2^{b2} & u_3^{b2} \end{bmatrix}^{\mathrm{T}}, \tag{100}$$

where $u_i = \dot{q}_i$. The dynamical model of the crane can be formulated following the procedure given in Sections 3 and 4, while the expressions for the determination of reaction forces are formulated as in Section 5.

6.2. Simulation results

In this section we implement the dynamical model of the crane numerically and present the simulations results. The parameters of the crane, which are used in the simulation are given in Table 1. The assumed modes for modeling the elasticity of the links are selected to be $\psi_i^{b1} = \sin(k_{1i}x)$ for Link 1 and $\psi_i^{b2} = \sin(k_{2i}x)$ for Link 2, where $i = 1, 2, 3$ and the values for $k_{11} = 0.314159$, $k_{12} = 0.628318$, $k_{13} = 0.942477$, and $k_{21} = 0.392699$, $k_{22} = 0.785398$, $k_{23} = 1.178097$.

Table 2
Geometric parameters of hydraulic cylinders.

Term	l_i^0	l_{pi}^0	l_{ri}^0	$s_{i,max}$	t_{pi}	y_{si}	y_{ei}
Value, m	3.6	0.05	3.37	3.32	0.03	0.05	0.10

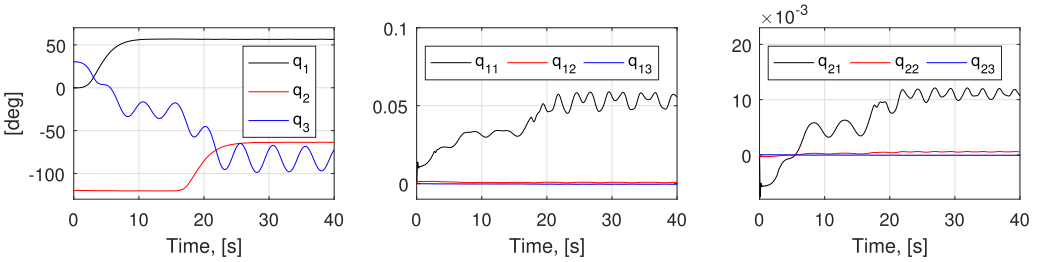

Fig. 7. Generalized coordinates of the crane.

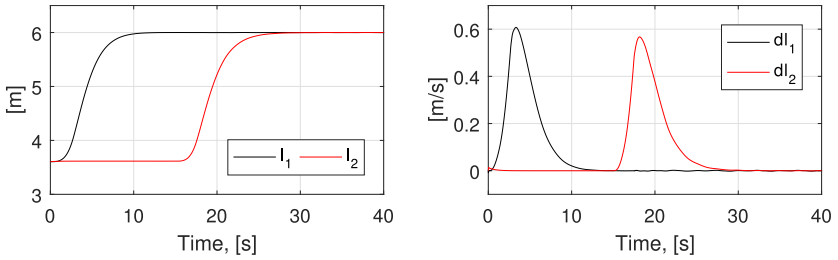

Fig. 8. The lengths and linear velocities of the cylinders.

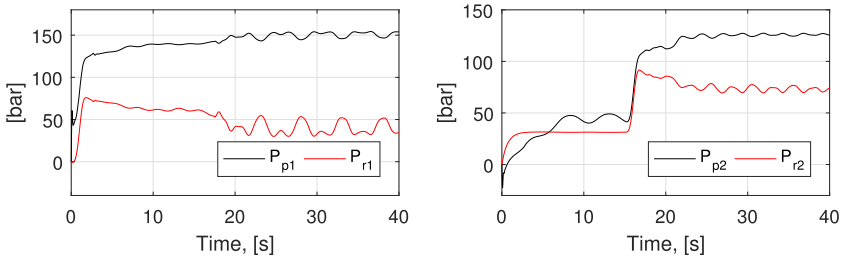

Fig. 9. Pressures in the cylinder chambers: P_{p1}, P_{r1} for cylinder 1 piston and rod sides, P_{p2}, P_{r2} for cylinder 2 piston and rod sides.

The crane is initialized in the undeformed position when the cylinder lengths are $l_1 = 3.606$ m, $l_2 = 3.606$ m, which corresponds to the following values of the generalized coordinate: $q_1 = 0$, $q_2 = -2/3\pi$, $q_3 = 1/6\pi$. The diagonal matrix of the damping coefficients is selected to be $\mathbf{D} = \text{diag}(0, 0, r_p, r_e, r_e, r_e, r_e, r_e, r_e)$, where $r_p = -5000$ and $r_e(t)$ is dependent on time as $r_e(t < 0.5\text{s}) = -250000$, while $r_e(t \geq 0.5\text{s}) = 0$. This means that the damping related to the elastic motion is only applied in the beginning of simulation to compensate for the motion caused by gravity forces applied at time $t = 0$ s. The desired values of the cylinder lengths are $l_{1d} = 6.00$ m and $l_{2d} = 6.00$ m. The parameters of the cylinder (as per Fig. 1), which are used in the simulation are given in Table 2. It is assumed that both cylinders are the same and the data is valid for $i = 1, 2$. The masses of the cylinder pistons and barrels are $m_p = 235$ kg and $m_b = 713$ kg. The area of the cylinder piston is $A_{pi} = 0.04524\text{m}^2$, the area on the rod side is $A_{ri} = 0.4241$ m^2, which corresponds to the piston diameter $d_{pi} = 0.24$ m and the rod diameter $d_{ri} = 0.06$ m. The bulk modulus of hydraulic oil is $\beta = 1.5 \cdot 10^9$ Pa, the density of hydraulic oil is $\rho = 880$ kg/m^3 and the internal leakage coefficient is $R_{li} = 10^{13}$. The discharge coefficient of the valve is $C_d = 0.6$, the relative orifice opening area is $w_i = 0.0007$ m^2. The gain for the flow controller (83) is selected to be $K_{v1} = 0.3$ for the cylinder 1 and $K_{v2} = 0.25$ for the cylinder 2. Additionally, we implement a low-pass filter to smoothen the input signal.

The values of generalized coordinates of the crane during the simulation are given in Fig. 7. The lengths of the cylinders and the rates of cylinder lengths are given in Fig. 8. The pressures in cylinder chambers are given in Fig. 9, where P_{p1}, P_{r1} are the pressures in cylinder 1 chambers on the piston and rod sides, and P_{p2}, P_{r2} are the pressures in cylinder 2 chambers on the piston and rod sides. The hydraulic flows into the cylinder chambers are given in Fig. 10, where Q_{p1}, Q_{r1} are the hydraulic flows into cylinder 1 chambers on the piston and rod sides, and Q_{p2}, Q_{r2} are the hydraulic flows into cylinder 2

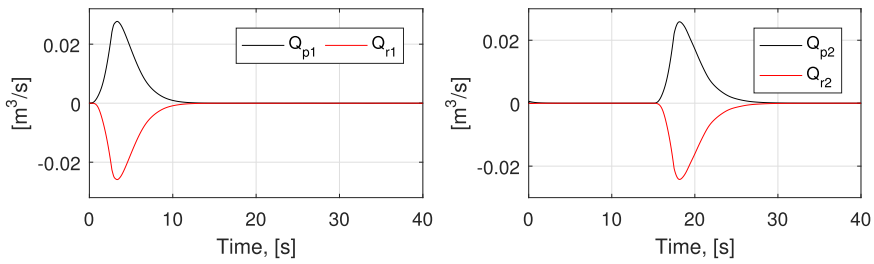

Fig. 10. Hydraulic oil flows into the cylinder chambers: Q_{p1}, Q_{r1} for cylinder 1 piston and rod sides, Q_{p2}, Q_{r2} for cylinder 2 piston and rod sides.

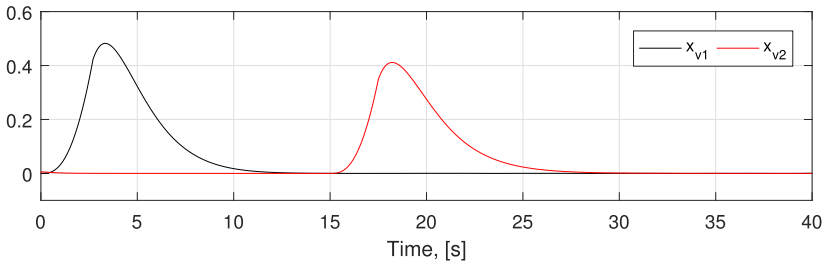

Fig. 11. Stroke of the valve: x_{v1} for cylinder 1, x_{v2} for cylinder 2.

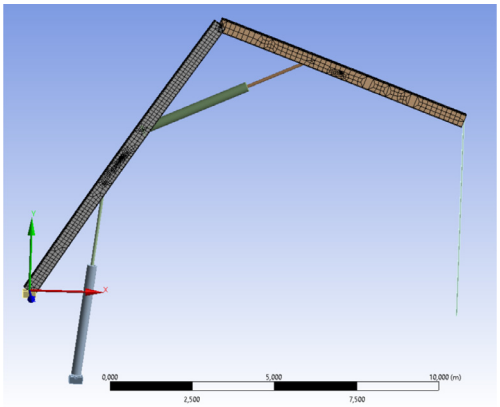

Fig. 12. ANSYS model of the planar knuckle boom crane used for validation.

chambers on the piston and rod sides. The strokes of the control valves are given in Fig. 11, where x_{v1} is the piston stroke of the control valve for cylinder 1, and x_{v2} is the piston stroke of the control valve for cylinder 2.

6.3. Validation of crane modeling assumptions

In this work we model elasticity of the beams using the assumed mode method, where the first three eigenmodes for a hinged-hinged uniform Euler–Bernoulli beam are included. The inertia of each cylinder is modeled as a lumped mass of a cylinder barrel and a lumped mass of a cylinder piston. The lumped masses are attached to the crane links through the spring-damper systems, where the spring stiffness is tuned to avoid significant relative motion, see Fig. 4. The cylinder forces are applied directly on the crane links. This way we avoid closed kinematic loops formed by the cylinders, which significantly simplifies the model and reduces the simulation time.

We validate the modeling assumptions by comparing the simulation results with the results obtained from the ANSYS finite element analysis of the same system, where the cylinders are included in the model, see Fig. 12. The ANSYS model has the same geometrical and mechanical properties as given in Section 6.2. The booms of the crane were modeled as flexible bodies, which were meshed with second order hexahedron elements (HEX20). The total number of elements in the model was 2478. The cylinders were modeled as rigid bodies, where the mass of barrels and pistons was the same as used in the BG analysis. The payload pendulum was modeled as a point mass attached to a rigid rod with negligible mass. All hinged joints between the bodies were modeled using Revolute Joint types, and sliding joints between the barrels and pistons of cylinders were modeled using Translational Joint types. Fixed boundary conditions were applied to two dummy blocks,

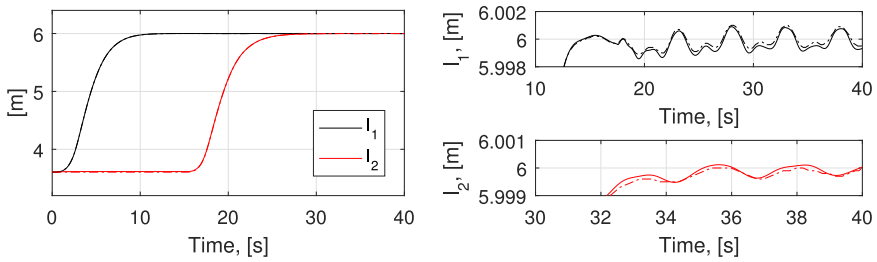

Fig. 13. Comparison of the cylinder lengths. Bond graph results are shown with solid lines, ANSYS results - with dashed lines. Graphs on the right-hand side are close-ups of the graph on the left-hand side.

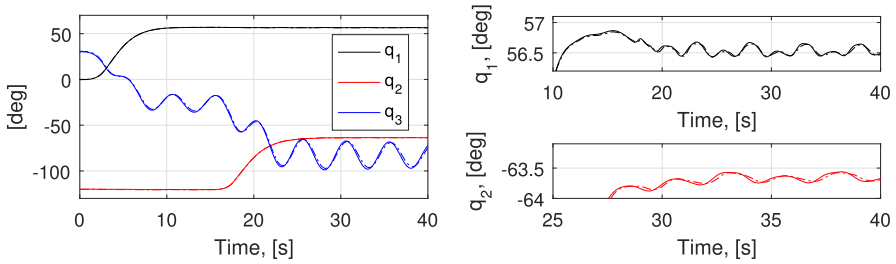

Fig. 14. Comparison of large motion degrees of freedom. Bond graph results are shown with solid lines, ANSYS results - with dashed lines. Graphs on the right-hand side are close-ups of the graph on the left-hand side.

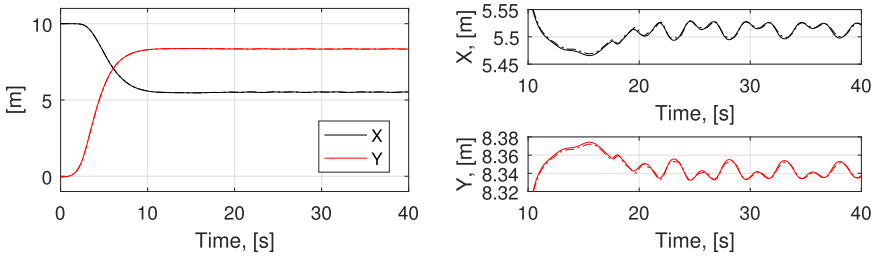

Fig. 15. Position of the end point of Link 1 given in the coordinates of the inertial frame. Bond graph results are shown with solid lines, ANSYS results - with dashed lines. Graphs on the right-hand side are close-ups of the graph on the left-hand side.

which were connected to the base of the inner boom and to the base of the inner cylinder by revolute joints. The simulation was executed using variable time stepping with the minimum time step of 1×10^{-7} s and the maximum time step of 0.2 s. The damping parameters were selected to be $\alpha = 0$ and $\beta = 0.02$. Since the aim of the validation is to validate the crane modeling assumptions, it is sufficient to model the mechanical part of the system and the modeling of hydraulics can be omitted. The rates of the cylinder lengths $\dot{l}_i$ obtained from the bond graph simulation (see Fig. 8) were used as input to the ANSYS model, which results in the equivalent actuation input in both models. In addition, acceleration of gravity was applied to all the bodies in the model.

The comparison of the time histories of the cylinder lengths is given is Fig. 13. The comparison of the degrees of freedom associated with large motion is given in Fig. 14. The elastic behavior is evaluated by comparison of the position of the end points of Link 1 and Link 2 given as x and y coordinates in the inertial frame. The position of the end point of Link 1 is given in Fig. 15, and the position of the end point of Link 2 is given in Fig. 16.

The comparison of the axial forces in the cylinders is given in Fig. 17. Results obtained in Figs. 13–17 show very good agreement and suggest that the dynamic behavior of the simplified model presented in this work agrees well with the behavior of the more complex FE model. Therefore, the modeling assumptions are considered to be reasonable.

6.4. Reaction forces

In this section we present time histories of reaction forces in the passive joints of the crane, which were determined by (97). The determined reaction forces are compared to the results obtained from the ANSYS analysis in Fig. 18. The terms ρ_1, ρ_2 are the reaction forces in Joint 1 given in the coordinates of Frame 1 along x and y axes. The terms ρ_3, ρ_4 are the reaction forces in Joint 2 given in the coordinates of Frame 2 along x and y axes. The terms ρ_5, ρ_6 are the reaction forces in

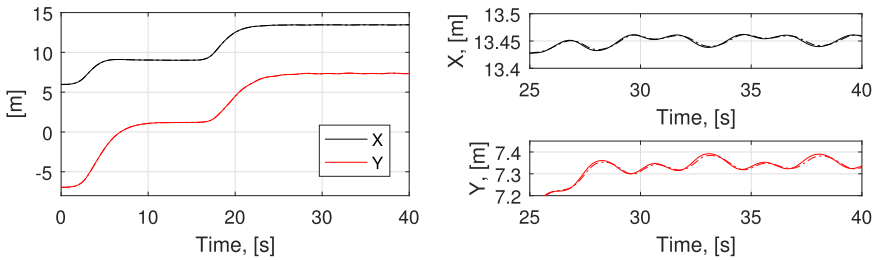

Fig. 16. Position of the end point of Link 2 given in the coordinates of the inertial frame. Bond graph results are shown with solid lines, ANSYS results - with dashed lines. Graphs on the right-hand side are close-ups of the graph on the left-hand side.

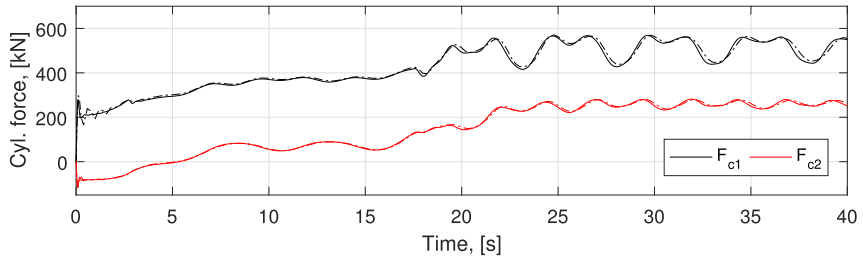

Fig. 17. Axial forces in the cylinders. Bond graph results are shown with solid lines, ANSYS results - with dashed lines.

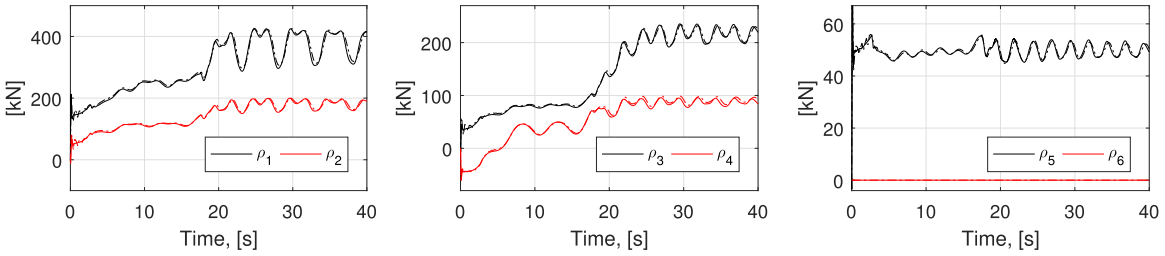

Fig. 18. Reaction forces ρ_1, ρ_2 in Joint 1, ρ_3, ρ_4 in Joint 2 and ρ_5, ρ_6 in the pendulum pivot joint. Bond graph results are shown with solid lines, ANSYS results - with dashed lines.

the pivot joint of the payload given in the coordinates of Frame 3 along x and y axes. The values of reaction forces obtained by (97) agree well with the results from the ANSYS analysis throughout the whole simulation.

7. Conclusions

In this work we have presented a procedure for the dynamic modeling of planar flexible manipulators, which are actuated by hydraulic cylinders. We have proposed a modeling framework, where both rigid body velocities and velocities associated with elastic motion are represented as twists. This led to a general and systematic procedure, where screw transformations were conveniently used for derivations. We have also demonstrated how dynamics of a manipulator can be coupled with dynamics of cylinders using the bond graph method. In addition, we have presented a procedure for the determination of reaction forces in passive joints of a manipulator, which was given as an extension of the dynamic modeling procedure.

We have implemented the presented procedures for a case of a planar model of a knuckle boom crane and studied dynamics of luffing motion of the crane. The modeling assumptions and simulation results were validated using the finite element analysis in ANSYS. We have also determined reaction forces in three passive joints and validated the values by the results from the ANSYS analysis. Both the elastic behavior and the values of reaction forces showed good agreement compared to the ANSYS results.

The advantage of the proposed method is that the proposed modeling assumptions significantly simplified the model. In particular, elimination of closed kinematic loops formed by hydraulic cylinders and derivation of closed-form kinematic relations between the cylinder lengths and joint rotation angles allowed for modeling the system as a minimal set of ODEs. In contrast to a set of DAE, which is a common way of modeling flexible systems with closed kinematic loops, a minimal formulation does not require inclusion of the constraint equations.

The proposed modeling and force analysis procedures can be a useful tool in design process of flexible mechanisms as well as in design and verification of hydraulic control systems. The future work is suggested to be an extension of the

proposed procedures for spatial flexible multibody systems. In addition, the presented formulation can be extended to include the joint clearance effect, joint flexibility, frictional effects and rub-impact loading.

Acknowledgment

The research presented in this paper has received funding from the Norwegian Research Council, SFI Offshore Mechatronics, project number 237896.

References

[1] E.M. Abdel-Rahman, A.H. Nayfeh, Z.N. Masoud, Dynamics and control of cranes: a review, Modal Anal. 9 (7) (2003) 863–908.
[2] S. Kilicslan, T. Balkan, S. Ider, Tipping loads of mobile cranes with flexible booms, J. Sound Vib. 223 (4) (1999) 645–657.
[3] B. Posiadała, Influence of crane support system on motion of the lifted load, Mech. Mach. Theory 32 (1) (1997) 9–20.
[4] A. Trabka, Dynamics of telescopic cranes with flexible structural components, Int. J. Mech. Sci. 88 (2014) 162–174.
[5] G. Sun, M. Kleeberger, Dynamic responses of hydraulic mobile crane with consideration of the drive system, Mech. Mach. Theory 38 (12) (2003) 1489–1508.
[6] F. Ju, Y. Choo, F. Cui, Dynamic response of tower crane induced by the pendulum motion of the payload, Int. J. Solids Struct. 43 (2) (2006) 376–389.
[7] R. Chen, L. Yan, Z. Jiao, Y. Shang, Dynamic modeling and analysis of flexible h-type gantry stage, J. Sound Vib. 439 (2019) 144–155.
[8] H.C. Pedersen, T.O. Andersen, B.K. Nielsen, Comparison of methods for modeling a hydraulic loader crane with flexible translational links, J. Dyn. Syst. Meas.Control 137 (10) (2015) 101012.
[9] G. Sun, J. Liu, Dynamic responses of hydraulic crane during luffing motion, Mech. Mach. Theory 41 (11) (2006) 1273–1288.
[10] A.A. Shabana, Dynamics of Multibody Systems, Cambridge university press, 2013.
[11] P.J. From, V. Duindam, K.Y. Pettersen, J.T. Gravdahl, S. Sastry, Singularity-free dynamic equations of vehicle–manipulator systems, Simul. Model. Pract. Theory 18 (6) (2010) 712–731.
[12] P.J. From, K.Y. Pettersen, J.T. Gravdahl, Singularity-free dynamic equations of spacecraft-manipulator systems, Acta Astronautica 69 (11–12) (2011) 1057–1065.
[13] B. Dasgupta, T. Mruthyunjaya, Closed-form dynamic equations of the general stewart platform through the newton–euler approach, Mech. Mach. Theory 33 (7) (1998) 993–1012.
[14] Y.-L. Hwang, Recursive newton–euler formulation for flexible dynamic manufacturing analysis of open-loop robotic systems, Int. J. Adv. Manuf.Technol. 29 (5) (2006) 598.
[15] T.R. Kane, D.A. Levinson, Dynamics, Theory and Applications, McGraw Hill, 1985.
[16] T. Kane, R. Ryan, A. Banerjee, Dynamics of a cantilever beam attached to a moving base, J. Guid. Control Dyn. 10 (2) (1987) 139–151.
[17] A. Cibicik, O. Egeland, Dynamic modelling and force analysis of a knuckle boom crane using screw theory, Mech. Mach. Theory 133 (2019) 179–194.
[18] A. Cibicik, G.O. Tysse, O. Egeland, Determination of reaction forces of a deck crane in wave motion using screw theory, ASME. J. Offshore Mech. Arct. Eng. (2019), doi:10.1115/1.4043701.
[19] W. Schiehlen, et al., Multibody Systems Handbook, 6, Springer, 1990.
[20] A. Cibicik, O. Egeland, Determination of constraint forces for an offshore crane on a moving base, in: 2018 5th International Conference on Control, Decision and Information Technologies (CoDIT), IEEE, 2018, pp. 233–240.
[21] M. Wojtyra, Joint reactions in rigid body mechanisms with dependent constraints, Mechanism and Machine Theory 44 (12) (2009) 2265–2278.
[22] F. Marques, A.P. Souto, P. Flores, On the constraints violation in forward dynamics of multibody systems, Multibody Syst. Dyn. 39 (4) (2017) 385–419.
[23] D.C. Karnopp, D.L. Margolis, R.C. Rosenberg, System Dynamics: Modeling, Simulation, and Control of Mechatronic Systems, John Wiley & Sons, 2012.
[24] T.K. Bera, A.K. Samantaray, Consistent bond graph modelling of planar multibody systems, World J. Model. Simul 7 (3) (2011) 173–178.
[25] A.A. Zeid, J.L. Overholt, Singularly perturbed formulation: explicit modeling of multibody systems, J. Franklin Inst. 332 (1) (1995) 21–45.
[26] A.M. Bos, Modelling multibody systems in terms of multibond graphs: with application to a motorcycle, PhD Thesis, Twente University, 1986 (1986).
[27] Y. Xing, E. Pedersen, T. Moan, An inertia-capacitance beam substructure formulation based on the bond graph method with application to rotating beams, J. Sound Vib. 330 (21) (2011) 5114–5130.
[28] V. Damic, M. Cohodar, Bond graph based modelling and simulation of flexible robotic manipulators, in: Proceedings 20th European Conference on Modelling and Simulation, Editors: Wolfgang Borutzky, Alessandra Orsoni, Richard Zobel© ECMS, 2006.
[29] R. Merzouki, A.K. Samantaray, P.M. Pathak, B.O. Bouamama, Intelligent Mechatronic Systems: Modeling, Control and Diagnosis, Springer Science & Business Media, 2012.
[30] T. Bera, A. Samantaray, R. Karmakar, Bond graph modeling of planar prismatic joints, Mech. Mach. Theory 49 (2012) 2–20.
[31] Y. Chu, L.I. Hatledal, V. Æsøy, S. Ehlers, H. Zhang, An object-oriented modeling approach to virtual prototyping of marine operation systems based on functional mock-up interface co-simulation, J. Offshore Mech. Arctic Eng. 140 (2) (2018) 021601.
[32] S.-J. Lee, P.-H. Chang, Modeling of a hydraulic excavator based on bond graph method and its parameter estimation, J. Mech. Sci. Technol. 26 (1) (2012) 195–204.
[33] V. Damic, M. Cohodar, M. Kulenovic, Modeling and simulation of hydraulic actuated multibody systems by bond graphs, Procedia Eng. 69 (2014) 203–209.
[34] B. Siciliano, L. Sciavicco, L. Villani, G. Oriolo, Robotics: Modelling, Planning and Control, 1st, Springer Publishing Company, Incorporated, 2008.
[35] R.M. Murray, Z. Li, S.S. Sastry, A Mathematical Introduction to Robotic Manipulation, CRC Press, 1994.
[36] J.M. McCarthy, G.S. Soh, Geometric Design of Linkages, 11, Springer Science & Business Media, 2010.
[37] J.K. Davidson, K.H. Hunt, Robots and Screw Theory: Applications of Kinematics and Statics to Robotics, Oxford University Press, 2004.
[38] H.E. Merritt, Hydraulic control systems, John Wiley & Sons, 1991.
[39] O. Egeland, J.T. Gravdahl, Modeling and Simulation for Automatic Control, 76, Marine Cybernetics Trondheim, Norway, 2002.
[40] O. Prakash, A.K. Samantaray, R. Bhattacharyya, Model-based multi-component adaptive prognosis for hybrid dynamical systems, Control Eng. Pract. 72 (2018) 1–18.
[41] V. Aesoy, E. Pedersen, Modeling and simulation for design and testing of direct injection gaseous fuel systems for medium-speed engines, SAE Int. J. Fuels Lubricants 4 (2) (2011) 188–203.